

Spray-Dried TiO₂(B)-Containing Photocatalytic Glass-Ceramic Nanobeads

Alessio Zandona,* Aurina Martínez Arias, Mirjam Gutbrod, Gundula Hensch, Alfred P. Weber, and Joachim Deubener

Glass-ceramic nanospheres of molar composition 0.83 SiO₂ · 0.17 TiO₂ are produced by the sol-gel spray-drying method followed by controlled heat treatments up to 1200 °C. TiO₂(B) and anatase nanocrystals are precipitated in the glassy matrix: the latter phase gradually predominates with increasing ceramization temperature and time, in parallel to an overall increase in crystal sizes. The nanospheres exhibit evident photocatalytic activity under UV-A irradiation, especially at annealing stages involving a comparatively higher amount of TiO₂(B) and smaller crystals. The occurrence of TiO₂(B) in this simplified binary glass-ceramic material underlines the key role of this phase in the dynamics of crystallizing TiO₂-bearing silicate melts.

In addition, photocatalytic glass-ceramics directly based on the formation of TiO₂-bearing functional crystals have been recently reported.^[12–17]

The above-pictured complexity of the role of Ti⁴⁺ for the formation and crystallization of silicate melts has not yet been balanced by an overarching scientific understanding of these processes. Thus, this study was conceived as a fundamental investigation of a representative simplified binary glass, to elucidate how TiO₂-bearing silicate glasses and glass-ceramics behave and react during thermal annealing. The

selected molar composition (0.83 SiO₂ · 0.17 TiO₂) exhibits high liquidus temperature and a strong tendency to crystallize,^[18] which are known to prevent the production of SiO₂-TiO₂ glasses by the conventional melt-quench route.^[19] The sample was therefore synthesized by the spray-drying method, mostly employed for food,^[20] drug delivery systems^[21,22] or ceramic nanoparticles^[23] processing and only limitedly explored for the development of functional glassy and glass-ceramic materials.^[24–28] On the whole, we additionally report a novel inexpensive method for the production of photocatalytic glass-ceramic nanobeads based on the crystallization of TiO₂(B) and anatase.

1. Introduction

The technological significance of TiO₂ in glasses and glass-ceramics is inextricably intertwined with the variable oxygen coordination of Ti⁴⁺ in silicate melts, which is compositionally dependent and described in terms of a broad distribution between: (fourfold) tetrahedral, (fivefold) square-based pyramidal and (sixfold) octahedral configurations.^[1–4] Acting as a low-coordinated glass former, Ti⁴⁺ enables inter alia the production of ultra-low-expansion titania-silica glass.^[4,5] Conversely, its strong tendency to increase its coordination number toward 6 during glass annealing^[6,7] has been exploited since the early days of glass-ceramics to control the devitrification process.^[8] In this case, an optimized heat treatment is typically employed to induce the precipitation of nanosized TiO₂-bearing nuclei, acting as nucleation sites for the subsequent crystallization of the desired functional phase(s) within the glass matrix.^[9] This procedure is still today essential for the production of, for instance, low-dielectric-loss cordierite glass-ceramics^[10] and zero-thermal-expansion lithium aluminosilicate glass-ceramics.^[11]


2. Results

An overview of the thermal behaviour of spray-dried and calcined SiTi17 was first obtained from a thermogravimetry/differential scanning calorimetry (TGA/DSC) measurement at 10 K min⁻¹ up to 1250 °C (Figure 1). The strong endothermic peak (*T*₁) occurring below 200 °C and coupled with a substantial mass loss (almost 10%) was most likely related to the desorption of water. The further slower mass loss up to 800 °C revealed that the preliminary calcination at 500 °C for 1 h had been insufficient to volatilize all the organic components still contained in the glass after spray-drying (in agreement with previous observations by other authors^[24]). The mass of the sample remained instead unchanged at a higher temperature, where three broad exothermic events (*T*₂, *T*₃, *T*₄) marked the onset of glass crystallization; the calorimetric signature of the glass transition (*T*_g) was barely visible as a subtle change in slope in the range 650–700 °C.

Hot-in hot-out ceramization protocols were applied to the calcined SiTi17 powder to obtain glass-ceramic nanobeads. X-ray diffraction (XRD) characterization (Figure 2) allowed to identify anatase [PDF 98-000-9852] and TiO₂(B) [PDF 98-004-1056] as the

A. Zandona, M. Gutbrod, Dr. G. Hensch, Prof. J. Deubener
Institute of Non-Metallic Materials
Clausthal University of Technology
Zehntnerstrasse 2A, 38678 Clausthal-Zellerfeld, Germany
E-mail: alessio.zandona@tu-clausthal.de

A. Martínez Arias, Prof. A. P. Weber
Institute of Particle Technology
Clausthal University of Technology
Leibnizstraße 19, 38678 Clausthal-Zellerfeld, Germany

 The ORCID identification number(s) for the author(s) of this article can be found under <https://doi.org/10.1002/adfm.202007760>.

© 2020 The Authors. Advanced Functional Materials published by Wiley-VCH GmbH. This is an open access article under the terms of the Creative Commons Attribution License, which permits use, distribution and reproduction in any medium, provided the original work is properly cited.

DOI: 10.1002/adfm.202007760

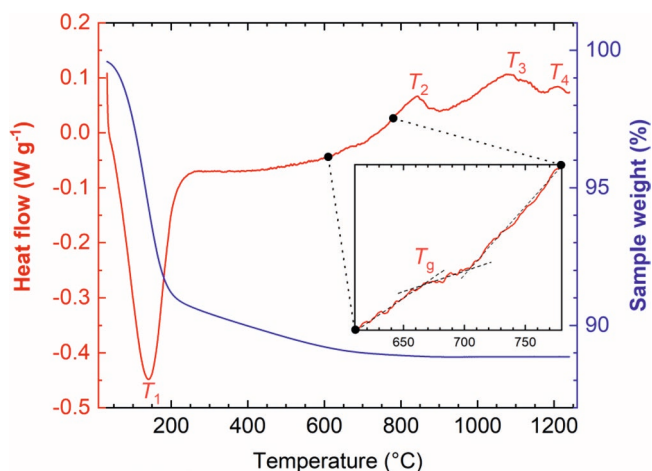


Figure 1. TGA (in blue) and DSC (in red) traces measured from sample SiTi17 during a simple upscan at 10 K min^{-1} (T_1 : endothermic water desorption; T_g : glass transition; T_2 , T_3 , T_4 : several exothermic crystallization events).

first crystalline phases forming in the initially amorphous material. The peaks related to the latter phase (see for instance the broad reflection at $\approx 58.5^\circ 2\theta$) appeared to weaken with increasing annealing temperature, while those of anatase underwent an evident sharpening suggesting a general increase in crystallite size. Moreover, the amorphous “hump” exhibited a shift to lower 2θ -angles, toward the position characteristic for glassy SiO_2 . At 1200°C , weak crystalline signatures related to rutile [PDF 98-000-9161] and cristobalite [PDF 98-000-9327] were also detected.

Raman spectroscopic measurements were employed to monitor the specific evolution of the TiO_2 polymorphs during the chosen heat treatments (Figure 3). Raman bands assignable to anatase and $\text{TiO}_2(\text{B})$ ^[29] appeared simultaneously already

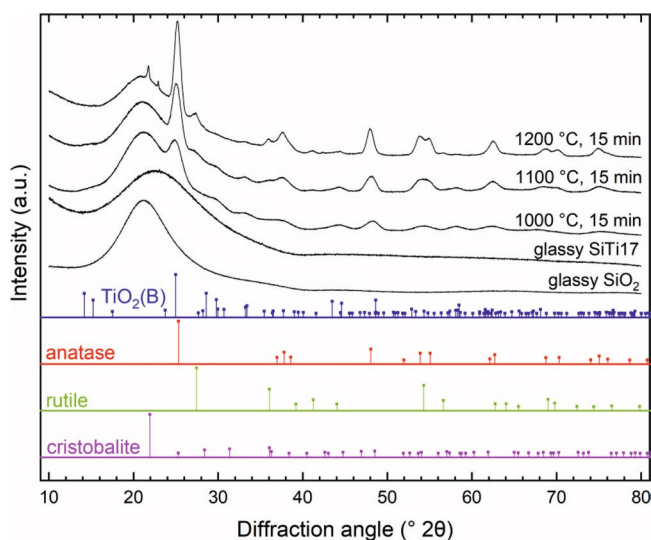


Figure 2. X-ray diffractograms of glassy SiTi17 (treated at 600°C for 10 h) and after various annealing stages, as well as of the glassy SiO_2 reference produced within this work. Reference cards for $\text{TiO}_2(\text{B})$ [PDF 98-004-1056], anatase [PDF 98-000-9852], rutile [PDF 98-000-9161], and low cristobalite [PDF 98-000-9327] are reported for comparison.

at 800°C and grew substantially with increasing ceramization temperature. The band (at $\approx 930 \text{ cm}^{-1}$) associated with low-coordinated Ti in the amorphous silicate network^[4,30] gradually reduced its intensity but never disappeared, suggesting a non-negligible solubility of Ti in SiO_2 (fairly stable technical glasses can be produced in the $\text{SiO}_2\text{-TiO}_2$ system at low TiO_2 loading^[19,31]). The bands related to anatase predominated in the spectra obtained from the samples treated at higher temperatures or for longer times, suggesting a faster growth of this phase with respect to $\text{TiO}_2(\text{B})$.

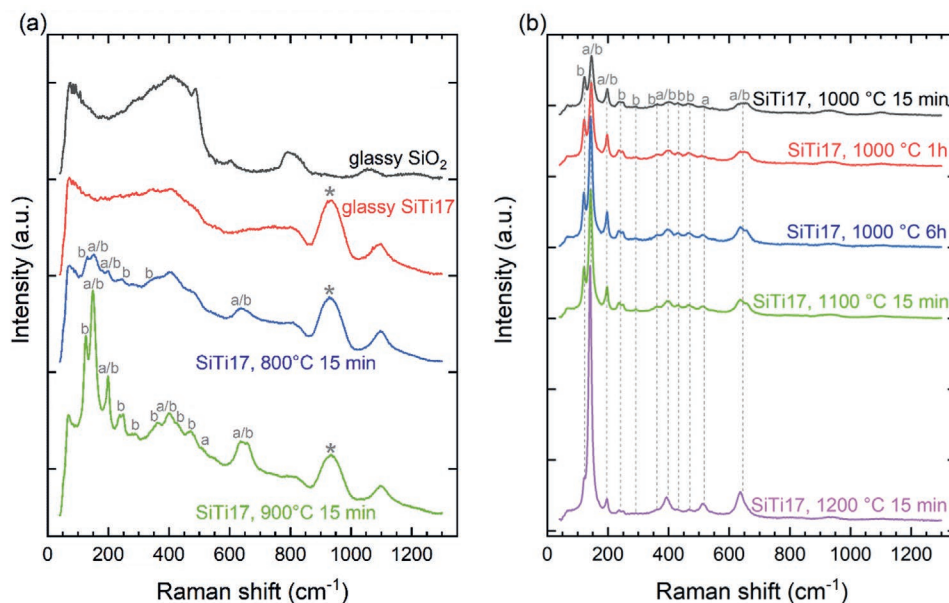


Figure 3. a) Raman spectra of glassy SiO_2 , glassy SiTi17 and SiTi17 nanospheres ceramized up to 900°C ; b) Raman spectra of SiTi17 nanospheres ceramized up to 1200°C (the symbol * labels the strongest band associated to Ti in the amorphous silicate network, while b and a-in gray- respectively mark all visible Raman bands of $\text{TiO}_2(\text{B})$ and anatase^[29] in the spectra).

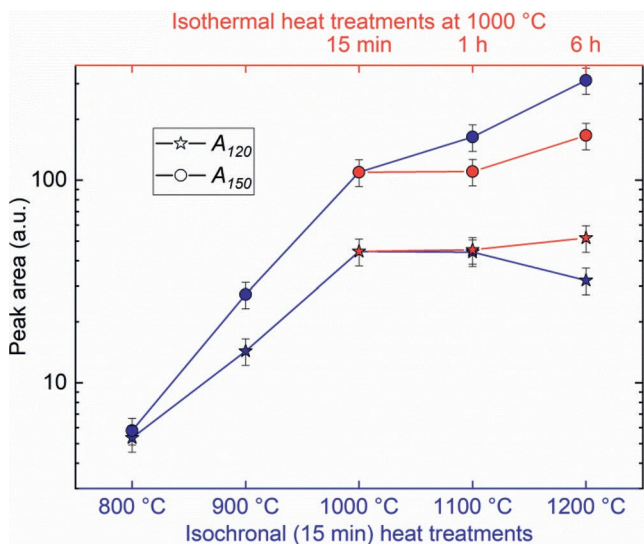


Figure 4. Peak areas obtained after fitting the main Raman bands of TiO₂(B) and anatase (A₁₂₀ and A₁₅₀, see the Experimental Section and ref. [29]) within the spectra reported in Figure 2a,b (mind the logarithmic scale of the vertical axis); blue data points refer to the isochronal sample series, red ones to the isothermal one.

Interpretation of the Raman spectra was supported by the fitting procedure described in the Experimental Section, evaluating changes in the area of the most intense bands of TiO₂(B) and anatase, respectively located at roughly 120 and 150 cm⁻¹ and accordingly labelled as A₁₂₀ and A₁₅₀. The signatures of both phases underwent a clear growth in Raman intensity with increasing ceramization temperature and time (Figure 4), although this phenomenon was far more pronounced for anatase. Indeed, the values computed for TiO₂(B) seemed to stagnate between 1000 °C and 1100 °C and displayed a slight drop at 1200 °C.

The morphology of some selected samples was subsequently characterized by transmission electron microscopy (TEM) (Figure 5). The powders were composed of mostly amorphous nanobeads, with a radius up to 100 nm. They contained a fine dispersion of crystalline nuclei, whose

radius increased with increasing ceramization temperature and time, from roughly 2–3 nm to 5–7 nm. The diameter of the primary nanospheres did not seem to perceptibly influence the size of the final TiO₂-bearing nanocrystals.

In fact, the small-angle X-ray scattering (SAXS) measurements performed on the samples (the raw experimental curves are available in Figure S1, Supporting Information) contained a characteristic “hump” in the Guinier region, manifesting the formation of nanosized objects. Data evaluation yielded the particle size distributions pictured in Figure 6 and detailed in Table 1 by the R20, R50, and R80 values (respectively corresponding to the radii defining the 20th, 50th, and 80th percentiles), relative standard deviations and surface-to-volume (S/V) ratios. The crystals generally appeared to grow in size with increasing temperatures and, to a minor extent, also with longer annealing at 1000 °C. This observation confirmed the crystal growth tendency qualitatively inferred from the above-described sharpening of XRD peaks (Figure 2).

Eventually, the photocatalytic activity of the glass-ceramic nanospheres was tested under UV-A irradiation. The decomposition of stearic acid (Figure 7a,b and Figure S2, Supporting Information) proceeded faster in the samples annealed at 1000 °C for 15 min and 1 h, while a longer annealing time (6 h) or a higher ceramization temperature (1100 °C) appeared to affect negatively the photocatalytic activity of the samples. The glassy materials displayed instead no relevant changes in the IR-bands of stearic acid in the studied time range. Concurrently, the estimation of the optical band gap E_g obtained from the UV–vis analysis hinted at a gradual decrease in band gap energy with increasing ceramization time and/or temperature: the results were 3.7(1) eV for glassy SiTi17, 3.4(1) eV for SiTi17 annealed at 1000 °C for 15 min, 3.2(1) eV after annealing at 1000 °C for 6 h and at 1100 °C for 15 min. Standard Degussa p25, measured as a reference, yielded $E_g = 3.0(1)$ eV, in line with previous literature sources.^[32,33]

3. Discussion

Formation of TiO₂(B) nanocrystals has been previously reported in amorphous SiO₂-TiO₂ thin films^[35] and lithium

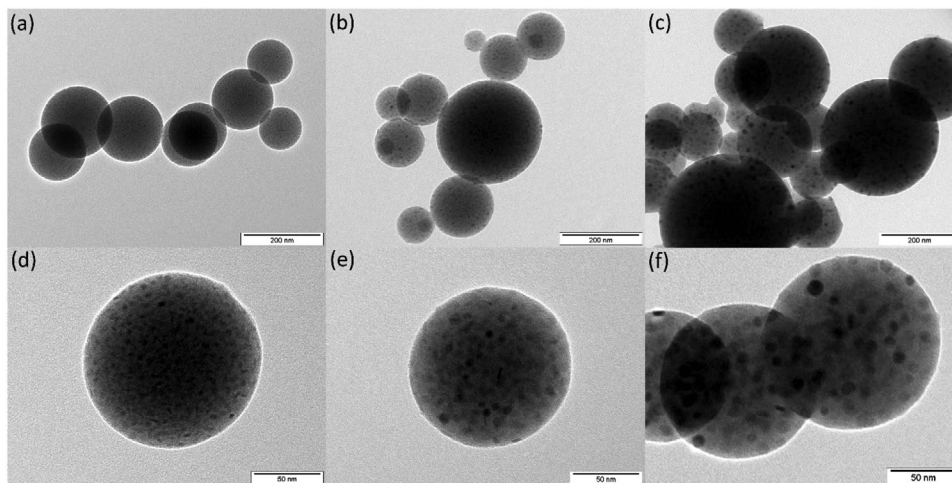


Figure 5. TEM micrographs of SiTi17 nanobeads, after annealing: a,d) at 1000 °C for 15 min, b,e) at 1000 °C for 6 h, c,f) at 1200 °C for 15 min.

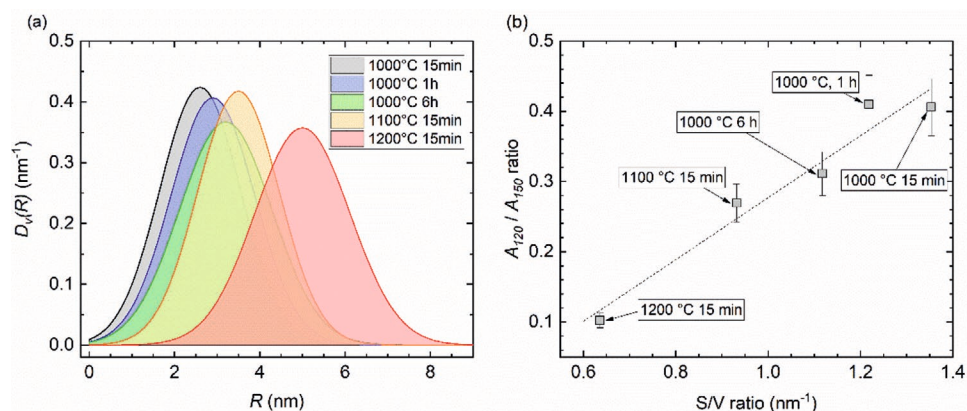


Figure 6. a) Volume-weighted particle size distribution $D_v(R)$ of the TiO_2 crystals formed in the SiTi17 nanospheres at various annealing stages, as extracted from the SAXS measurements (raw data in Figure S1, Supporting Information) using a Gaussian approximation; b) correlation between the A_{120}/A_{150} ratio, computed after fitting the main Raman bands of $\text{TiO}_2(\text{B})$ and anatase (see in Experimental Section and Figure 4), and the mean surface-to-volume (S/V) ratio of the TiO_2 crystals obtained from the SAXS data evaluation.

aluminosilicate glass-ceramics.^[29] Its observation also within this work supports a strong link between glass crystallization and this rather rare monoclinic TiO_2 polymorph, first synthesized from hydrolyzed alkali titanates.^[36] Its structure has been modelled in terms of two different Ti sites, an octahedral one and a more distorted one, approaching a square-pyramidal five-coordinated configuration.^[37,38] This latter arrangement is also very frequent for Ti^{4+} in silicate glasses,^[2,4] so that it is not implausible that $\text{TiO}_2(\text{B})$ might effectively serve as a “bridging phase” between the amorphous structure of the initial glass and the regular octahedral oxygen coordination encountered in anatase and rutile.^[39] Similarly, the density of $\text{TiO}_2(\text{B})$ is lower than that of anatase^[36] and therefore closer to the one of the parent glass. All in all, the mechanistic interpretation of TiO_2 crystallization in silicate glasses according to Ostwald’s rule of stages^[40] proposed in a recent publication^[29] is fortified by the results of this work.

Since both $\text{TiO}_2(\text{B})$ and anatase underwent contemporary changes in their total amount, crystal structure, crystallite size, and degree of crystallinity during ceramization, a quantitative treatment of the Raman signals proved rather challenging. Nevertheless, the two phases were found to coexist with each other already at 800 °C and up to 1200 °C. TEM micrographs and SAXS results reveal in all samples generally monodispersed nuclei, inhibiting unambiguous pinpointing of the two TiO_2 polymorphs as separate crystals. All these considerations appear to discredit a simple linear evolution involving amorphous TiO_2 demixing, initial crystallization of $\text{TiO}_2(\text{B})$, and a subsequent transformation into anatase.

In turn, the Raman A_{120}/A_{150} ratios correlate fairly well with the S/V ratios extracted from the SAXS measurements (Figure 6b). While single-phase $\text{TiO}_2(\text{B})$ crystals could only be obtained in glass-ceramics in the form of thin nanoplatelets,^[29] thin $\text{TiO}_2(\text{B})$ layers have been also identified on the surface of anatase nanofibers^[41] or as lamellae in natural anatase crystals.^[42] All these observations designate a crucial role of the S/V ratio of the crystals in determining the occurrence of $\text{TiO}_2(\text{B})$, in direct analogy with the higher thermodynamic stability of anatase in the form of nanocrystals with respect to rutile, predicted theoretically and inferred experimentally in the past.^[43–46] Concerning the results of this work, it is indeed possible to hypothesize the formation of TiO_2 crystals possessing an anatase core and a $\text{TiO}_2(\text{B})$ shell, marking the contact with the enclosing SiO_2 -enriched amorphous matrix. The Raman signature belonging to the shell would then predominate in early annealing stages because of the very small size (and high S/V ratio) of the crystals, progressively weakening as the crystals grow. The two possible interpretations of the crystallization sequence are summarized in Figure 8.

Although the functional $\text{TiO}_2(\text{B})$ and anatase crystals produced in this work are enclosed by a SiO_2 -enriched amorphous matrix, they clearly exhibit a photocatalytic response. The determined optical band gaps E_g appeared to decrease at higher annealing temperature and time, probably because of the general increase in crystallinity and crystal size, as known from previous literature.^[47,48] However, the photocatalytic activity was more intense in the samples containing smaller crystals (SiTi17 annealed at 1000 °C for 15 min and 1 h), suggesting a

Table 1. Some representative values for the volume-weighted particle size distribution $D_v(R)$ of the TiO_2 nanocrystals formed at various annealing stages in the SiTi17 nanospheres, as extracted from the SAXS measurements (S/V stands for the mean surface-to-volume ratio).

| Temperature [°C] | Time [min] | R20 [nm] | R50 [nm] | R80 [nm] | Relative standard deviation [%] | S/V ratio [nm ⁻¹] |
|------------------|------------|----------|----------|----------|---------------------------------|-------------------------------|
| 1000 | 15 | 1.8 | 2.6 | 3.4 | 36.17 | 1.3538 |
| 1100 | 15 | 2.7 | 3.5 | 4.4 | 27.27 | 0.9318 |
| 1200 | 15 | 4.1 | 5 | 5.9 | 22.33 | 0.6361 |
| 1000 | 60 | 2.1 | 2.9 | 3.7 | 33.81 | 1.2188 |
| 1000 | 360 | 2.3 | 3.2 | 4 | 33.97 | 1.1176 |

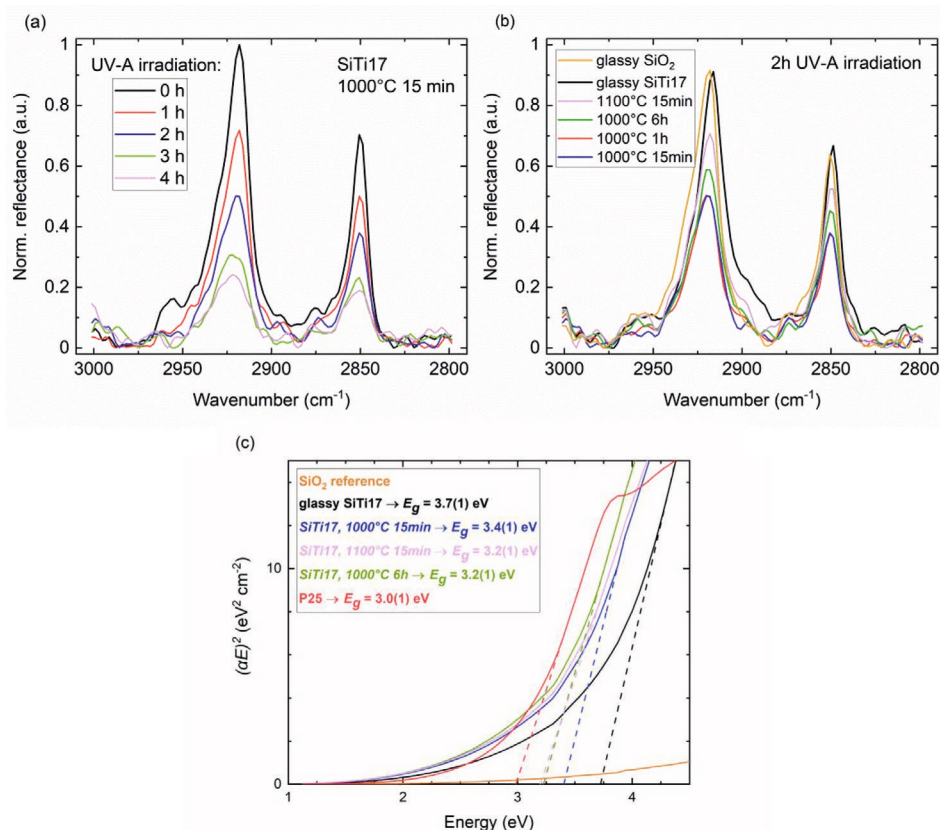


Figure 7. a) Normalized IR reflectance in the spectral range 3000–2800 cm⁻¹, from measurements performed during photocatalytic testing of sample SiTi17 annealed at 1000 °C for 15 min; b) a similar plot comparing all samples after 2 h UV-A irradiation; c) Tauc plots^[34] for the SiO₂ reference, SiTi17 (glassy and after annealing) and Degussa p25, with the obtained optical band gap E_g values (the raw extinction spectra are provided as Figure S3, Supporting Information).

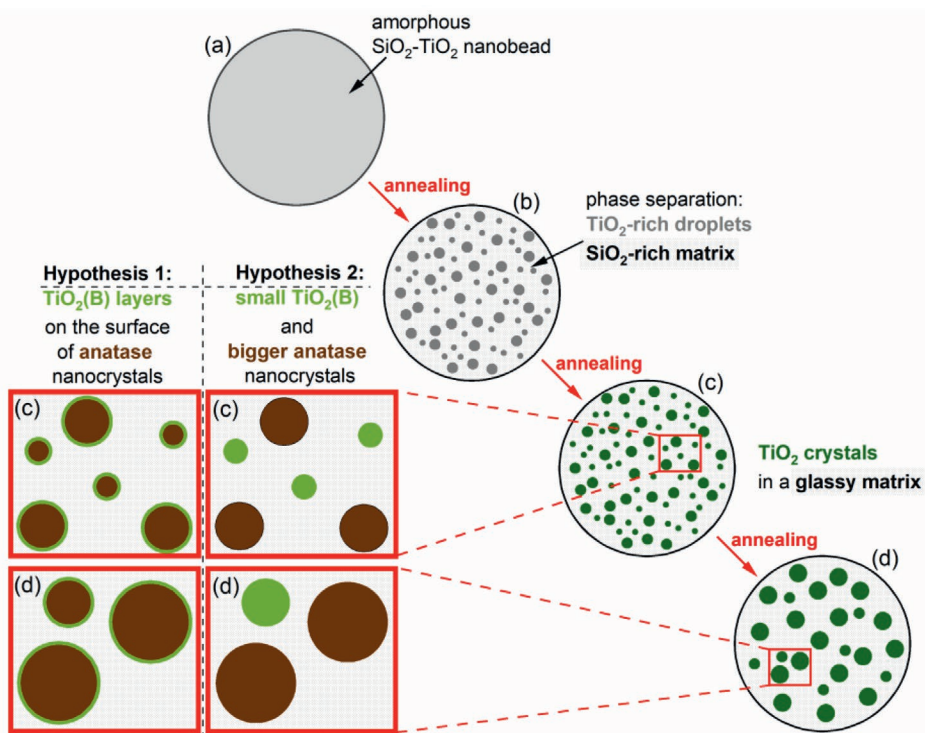


Figure 8. Schematization of the crystallization process taking place in the analysed SiTi17 glassy nanobeads, with the two proposed hypotheses for the coexistence of TiO₂(B) and anatase nanocrystals in the samples.

predominance of the active surface area over the (slight) band gap broadening in determining the quantum efficiency. The possibility of incipient partial sintering of the nanospheres at high temperatures (1100 °C and 1200 °C), affecting their dispersion during the dip-coating (as mentioned in the Experimental Section), should also not be overlooked in this regard. It is then clear that the mutual spatial relations between the TiO₂(B) and anatase crystals in the samples might be decisive, as heterojunctions between different TiO₂ polymorphs have been shown to noticeably enhance their ability to decompose organic matter under UV-A irradiation.^[41,49–51] However, as discussed above, the available data do not allow to unambiguously identify the nanostructural arrangement of the two polymorphs, so that further investigations will be necessary to determine the actual photocatalytic mechanism of this material.

Even considering the relatively low TiO₂ loading, possibly affecting the photocatalytic “gross performance” with respect to full TiO₂ materials,^[41,49–51] the nanobeads synthesized within this work certainly provide an alternative approach for the design of UV-A active materials, with a possible impact reaching far beyond the fundamental scope of this study.

4. Conclusion

Glassy nanospheres of SiO₂-TiO₂ composition were produced by sol-gel spray-drying and turned into glass-ceramics by controlled heat treatments. TiO₂(B)/anatase nuclei formed in the glass matrix, endowing photocatalytic activity to the material. The occurrence and central role of TiO₂(B) during the crystallization of silicate melts could be confirmed by the results of this study.

5. Experimental Section

Materials: Tetraethoxysilane (TEOS, 99.0% (GC), Fluka) and titanium (IV) butoxide (97.0%, Sigma-Aldrich), were used as precursors for the synthesis of the SiO₂-TiO₂ glassy nanobeads. They were solved in isopropanol (99.0%, Carl Roth). 1 M nitric acid (ORG Laborchemie GmbH) and ethyl acetoacetate (99.0%, Sigma-Aldrich) were respectively used as a promoter for the hydrolysis of TEOS and as a stabilizer for Ti-butoxide. All chemicals were employed as received.

Sample Preparation: For the sol-gel preparation of the nanobeads, two different solutions were prepared and subsequently mixed together. Solution 1 was prepared from TEOS, isopropanol, deionized water, which was used as a hydrolysis agent, and 1 M nitric acid; pH was adjusted to ≈1 and the molar ratio of TEOS to H₂O was set to 0.25. Parallel, solution 2 was prepared by mixing equimolar amounts of Ti-butoxide and ethyl acetoacetate in isopropanol. Both solutions were diluted with isopropanol targeting a concentration of 0.1 mol TEOS or Ti-butoxide per 120 g solution. At room temperature and under continuous agitation with a magnetic stirrer, both mixtures were first homogenized separately and then solution 2 was added to solution 1 in the required composition, namely 0.83 SiO₂ · 0.17 TiO₂ (hereafter SiTi17).

The resulting mixture was spray-dried to produce the desired nanospheres. The experimental setup consisted of an aerosol atomizer (Atomizer, AGK 2000, Palas) operated with pressurized air (2.8 bar) as carrier gas, a tube furnace set at 200 °C and a particle filter. The atomized solution was dried in the tube furnace with a residence time of 1.6 s. During this stage, the evaporation of the solvent induced a droplet self-assembly process, leading to spherical dry particles. Moreover, both

precursors (TEOS and Ti-Butoxide) started to decompose, yielding a homogeneous amorphous SiO₂-TiO₂ mixture. Pure SiO₂ nanospheres were prepared to be used as reference by spray-drying pure solution 1.

After collecting the dried nanobeads from the filter, they were pre-emptively calcined at 500 °C for 1 h to decompose the organic precursors. After this, they were subjected to hot-in hot-out crystallization protocols,^[29] placing them in a hot furnace and rapidly quenching them in air at the end of an isothermal hold. In this way, an isochronal sample series (15 min at 800 °C, 900 °C, 1000 °C, 1100 °C or 1200 °C) and an isothermal one (15 min, 1 h or 6 h at 1000 °C) were produced. For the obtainment of glassy SiTi17, the calcined powder was additionally annealed at 600 °C for 10 h, to remove all remnant organic matter. The SiO₂ reference was instead directly subjected to a heat treatment at 1000 °C for 15 min after the preliminary calcination at 500 °C.

TGA/DSC: A simple upscan at 10 K min⁻¹ was performed on a TGA/DSC 3+ (Mettler-Toledo), using a lidded PtRh20 crucible containing 36.7 mg of the pre-emptively calcined SiTi17 sample. The measurement was run in N₂ atmosphere (≥99.999%, flow rate 60 ml min⁻¹).

X-Ray Diffraction (XRD): The measurements were performed on a Panalytical Empyrean diffractometer, operated at 40 kV 40 mA⁻¹ and equipped with a Cu X-ray tube, an adjustable x-y-z platform with powder sample holder and a PIXcel 1D detector (255 channels, 14 mm active length). The data were collected in the range 10–80 °2θ, with a step size of 0.013 °2θ and 2700 s per step.

Raman Spectroscopy: The spectroscopic characterization was performed on a Bruker Senterra confocal Raman microscope equipped with a frequency-doubled Nd/YAG laser (532 nm). The spectra were collected at a power of 5 mW, with an integration time of 15 s and two accumulations in the range 40–1550 cm⁻¹. The obtained data were evaluated according to the procedure already described elsewhere:^[29] the spectra were normalized to the intensity at the edge filter of the spectroscope (75 cm⁻¹) and then a spline interpolation through set points was used to approximate the glass spectrum in the range 80–250 cm⁻¹. The main bands of TiO₂(B) (at ≈120 cm⁻¹) and anatase (at ≈150 cm⁻¹) were subsequently fitted with Gaussian peaks; the respective peak areas A₁₂₀ and A₁₅₀ and their ratio were employed to assess semi-quantitatively their growth during the heat treatments.

Transmission Electron Microscopy (TEM): A small amount of heat-treated SiTi17 nanospheres (1000 °C – 15 min, 1000 °C – 6 h, and 1200 °C – 15 min) was loaded on a carbon-coated copper grid and measured in a JEOL JEM2100 TEM, operated at 160 kV in bright-field mode.

Small-Angle X-Ray Scattering (SAXS): The characterization took place on the above-described diffractometer, re-equipped with a SAXS stage and operated at 45 kV 40 mA. The SiTi17 powders were loaded in metallic sample holders between two Mylar foils and measured in the range –0.115–5 °2θ, with a step size of 0.01 °2θ and 2.2 s per step. The SiO₂ reference was also measured as background for the subsequent data evaluation, performed automatically using the software EasySAXS (Panalytical). After background subtraction, the volume-weighted particle size distribution D_v(R) of the TiO₂ crystals could be obtained from the scattering curves using a Gaussian approximation, under the assumption (supported by the TEM micrographs) of monodispersed, internally homogeneous and non-interacting spherical nuclei.

Photocatalytic Activity and UV-Vis Analysis: Representative samples were selected for photocatalytic testing: glassy SiO₂, glassy SiTi17, SiTi17 annealed at 1000 °C for 15 min, 1 h, 6 h, and at 1100 °C for 15 min. SiTi17 treated at 1200 °C for 15 min had undergone partial particle sintering that prevented its effective dispersion in isopropanol; standard Degussa p25 TiO₂ powder was also tested as a means of comparison. The nanospheres were suspended (1 wt%) in isopropanol and dip-coated on borosilicate glass plates, repeating the procedure five times with a drawing speed of 2 mm s⁻¹. Subsequently, a 0.5 wt% stearic acid (C₁₈H₃₆O₂) isopropanol solution was deposited once over the samples by dip-coating at 1 mm s⁻¹. Photocatalytic degradation of this compound occurred due to UV-A irradiation (120 W m⁻²) under Philips lamps (Cleo Performance 40-W-R); the process was monitored by spectroscopic measurements after 10 min, 1 h, 2 h, 3 h, and 4 h, targeting the IR-active vibrational bands of stearic acid located in the range 3000–2800 cm⁻¹.^[52]

The measurements were performed in grazing incidence reflection geometry on a Bruker Vertex 70 FT-IR spectrometer. Degussa p25 was able to decompose the stearic acid already after 10 min irradiation, confirming the applicability of our experimental setup. To highlight intensity variations in the spectra obtained from the samples, a straight baseline was subtracted in the mentioned range and the peak intensity at $t = 0$ was normalized to 1. The results are shown for the “atmosphere side” of the dip-coated borosilicate plates, although no relevant difference could be discerned compared to their “tin bath side”.

An estimation of the optical band gap E_g of glassy SiTi17 and of the samples annealed at 1000 °C for 15 min and 6 h and at 1100 °C for 15 min was obtained applying the procedure described by Tauc.^[34] Extinction spectra were collected in the UV–vis range (190–1100 nm) in 5 nm steps using a Specord 200 spectrometer (Analytik Jena). The nanobeads were suspended in isopropanol (0.01 wt%) for the measurements. The applicability of this procedure was tested with a suspension of standard Degussa p25 TiO₂ powder (0.0025 wt%) in isopropanol.

Supporting Information

Supporting Information is available from the Wiley Online Library or from the author.

Acknowledgements

A.Z. is grateful to the Deutsche Forschungsgemeinschaft for providing funding for this research through the Walter-Benjamin-Scholarship, grant n. ZA 1188/1-1. The authors would also like to express their gratitude to Dr. Masoom Shaban for the fruitful discussions concerning the analysis of the photocatalytic activity of the samples.

Open access funding enabled and organized by Projekt DEAL.

Conflict of Interest

The authors declare no conflict of interest.

Keywords

glass-ceramics, nanotechnology, photocatalysis, sol-gel, spray-drying, TiO₂

Received: September 11, 2020

Revised: November 2, 2020

Published online: November 20, 2020

- [1] D. B. Dingwell, E. Paris, F. Seifert, A. Mottana, C. Romano, *Phys. Chem. Minerals* **1994**, *21*, 501.
- [2] F. Farges, G. E. Brown, A. Navrotsky, H. Gan, J. J. Rehr, *Geochim. Cosmochim. Acta* **1996**, *60*, 3039.
- [3] L. Cormier, P. H. Gaskell, G. Calas, J. Zhao, A. K. Soper, *Phys. B* **1997**, *234–236*, 393.
- [4] G. S. Henderson, X. Liu, M. E. Fleet, *Phys. Chem. Miner.* **2002**, *29*, 32.
- [5] D. R. Sandstrom, F. W. Lytle, P. S. P. Wei, R. B. Gregor, J. Wong, P. Schultz, *J. Non-Cryst. Solids* **1980**, *41*, 201.
- [6] O. S. Dymshits, A. A. Zhilin, V. I. Petrov, M. Ya. Tsender, T. I. Chuvaeva, V. V. Golubkov, *Glass Phys. Chem.* **1998**, *24*, 79.
- [7] L. Cormier, O. Dargaud, N. Menguy, G. S. Henderson, M. Guignard, N. Trcera, B. Watts, *Cryst. Growth & Des.* **2011**, *11*, 311.
- [8] S. D. Stookey, *Ind. Eng. Chem.* **1959**, *51*, 805.
- [9] J. Deubener, M. Allix, M. J. Davis, A. Duran, T. Höche, T. Honma, T. Komatsu, S. Krüger, I. Mitra, R. Müller, S. Nakane, M. J. Pascual, J. W. P. Schmelzer, E. D. Zanotto, S. Zhou, *J. Non-Cryst. Solids* **2018**, *501*, 3.
- [10] G. H. Beall, *Annu. Rev. Mater. Sci.* **1992**, *22*, 91.
- [11] *Low Thermal Expansion Glass Ceramics* (Eds: D. Krause, H. Bach), Springer-Verlag, Berlin **1995**.
- [12] T. Yazawa, F. Machida, K. Oki, A. Mineshige, M. Kobune, *Ceram. Int.* **2009**, *35*, 1693.
- [13] J. Fu, *Mater. Res. Bull.* **2011**, *46*, 2523.
- [14] J. Fu, *Mater. Lett.* **2012**, *68*, 419.
- [15] J. Fu, *Mater. Lett.* **2014**, *118*, 84.
- [16] V. Thakur, H. S. Kushwaha, A. Singh, R. Vaish, R. Punia, L. Singh, *J. Non-Cryst. Solids* **2015**, *428*, 197.
- [17] H. Masai, H. Sakurai, A. Koreeda, Y. Fujii, T. Ohkubo, T. Miyazaki, T. Akai, *Sci. Rep.* **2020**, *10*, 11615.
- [18] R. W. Ricker, F. A. Hummel, *J. Am. Ceram. Soc.* **1951**, *34*, 271.
- [19] P. C. SCHULTZ, *J. Am. Ceram. Soc.* **1976**, *59*, 214.
- [20] A. Gharsallaoui, G. Roudaut, O. Chamin, A. Voilley, R. Saurel, *Food Res. Int.* **2007**, *40*, 1107.
- [21] C. Arpagaus, A. Collenberg, D. Rütli, E. Assadpour, S. M. Jafari, *Int. J. Pharm.* **2018**, *546*, 194.
- [22] J. Poostforooshan, S. Belbekhouche, M. Shaban, V. Alphonse, D. Habert, N. Bousserhine, J. Courty, A. P. Weber, *ACS Appl. Mater. Interfaces* **2020**, *12*, 6885.
- [23] A. M. Arias, A. P. Weber, *J. Aerosol Sci.* **2019**, *131*, 1.
- [24] A. Douy, P. Canale, J. Coutures, *J. Eur. Ceram. Soc.* **1992**, *9*, 373.
- [25] I. Jaymes, A. Douy, *J. Am. Ceram. Soc.* **1992**, *75*, 3154.
- [26] G. Molino, A. Bari, F. Bains, S. Fiorilli, C. Vitale-Brovarone, *J. Mater. Sci.* **2017**, *52*, 9103.
- [27] P. Korteesuo, M. Ahola, M. Kangas, I. Kangasniemi, A. Yli-Urpo, J. Kiesvaara, *Int. J. Pharm.* **2000**, *200*, 223.
- [28] S. A. Saadaldin, A. S. Rizkalla, *Dent. Mater. J.* **2014**, *30*, 364.
- [29] A. Zandona, C. Patzig, B. Rüdinger, O. Hochrein, J. Deubener, *J. Non-Cryst. Solids: X* **2019**, *2*, 100025.
- [30] M. C. Tobin, T. Baak, *J. Opt. Soc. Am.* **1968**, *58*, 1459.
- [31] O. V. Mazurin, V. K. Leko, L. A. Komarova, *J. Non-Cryst. Solids* **1975**, *18*, 1.
- [32] X. Chen, L. Liu, P. Y. Yu, S. S. Mao, *Science* **2011**, *331*, 746.
- [33] J. F. Guayaquil-Sosa, B. Serrano-Rosales, P. J. Valadés-Pelayo, H. de Lasa, *App. Catal., B* **2017**, *211*, 337.
- [34] J. Tauc, *Mater. Res. Bull.* **1968**, *3*, 37.
- [35] T. Kogure, T. Umezawa, Y. Kotani, A. Matsuda, M. Tatsumisago, T. Minami, *J. Am. Ceram. Soc.* **2004**, *82*, 3248.
- [36] R. Marchand, L. Brohan, M. Tournoux, *Mater. Res. Bull.* **1980**, *15*, 1129.
- [37] M. Ben Yahia, F. Lemoigno, T. Beuvier, J.-S. Filhol, M. Richard-Plouet, L. Brohan, M.-L. Doublet, *J. Chem. Phys.* **2009**, *130*, 204501.
- [38] A. Vittadini, M. Casarin, A. Selloni, *J. Phys. Chem. C* **2009**, *113*, 18973.
- [39] F. Farges, G. E. Brown, J. J. Rehr, *Geochim. Cosmochim. Acta* **1996**, *60*, 3023.
- [40] W. Ostwald, *Z Phys. Chem. (N F)* **1897**, *22U*, 289.
- [41] W. Li, C. Liu, Y. Zhou, Y. Bai, X. Feng, Z. Yang, L. Lu, X. Lu, K.-Y. Chan, *J. Phys. Chem. C* **2008**, *112*, 20539.
- [42] J. F. Banfield, D. R. Veblen, D. J. Smith, *Am. Mineral.* **1991**, *76*, 343.
- [43] J. F. Banfield, B. L. Bischoff, M. A. Anderson, *Chem. Geol.* **1993**, *110*, 211.
- [44] H. Zhang, J. F. Banfield, *J. Mater. Chem.* **1998**, *8*, 2073.
- [45] T. B. Ghosh, S. Dhabal, A. K. Datta, *J. Appl. Phys.* **2003**, *94*, 4577.
- [46] A. S. Barnard, P. Zapol, *Phys. Rev. B* **2004**, *70*, 235403.
- [47] S. Lee, I.-S. Cho, J.-H. Noh, K. S. Hong, G. S. Han, H. S. Jung, S. Jeong, C. Lee, H. Shin, *Phys. Status Solidi A* **2010**, *207*, 2288.
- [48] L. Kavan, T. Stoto, M. Graetzel, D. Fitzmaurice, V. Shklover, *J. Phys. Chem.* **1993**, *97*, 9493.
- [49] B. Liu, A. Khare, E. S. Aydil, *ACS Appl. Mater. Interfaces* **2011**, *3*, 4444.
- [50] Z. Wang, Y. Wang, W. Zhang, Z. Wang, Y. Ma, X. Zhou, *J. Phys. Chem. C* **2019**, *123*, 1779.
- [51] J. Zhang, Q. Xu, Z. Feng, M. Li, C. Li, *Angew. Chem.* **2008**, *120*, 1790.
- [52] G. Hensch, J. Deubener, *Solar Energy* **2012**, *86*, 831.